Anionic Constitution of 1-Atmosphere Silicate Melts: Implications for the Structure of Igneous Melts

Abstract. *A structural model is proposed for the polymeric units in silicate melts quenched at 1 atmosphere. The anionic units that have been identified by the use of Raman spectroscopy are SiO_4^{4-} monomers, $Si_2O_7^{6-}$ dimers, SiO_3^{2-} chains or rings, $Si_2O_5^{2-}$ sheets, and SiO_2 three-dimensional units. The coexisting anionic species are related to specific ranges of the ratio of nonbridging oxygens to tetrahedrally coordinated cations (NBO/Si). In melts with $2.0 < NBO/Si < \sim 4.0$, the equilibrium is of the type $Si_2O_7^{6-} \rightleftarrows SiO_4^{4-} + SiO_3^{2-}$. In melts with NBO/Si ~ 1.0 to 2.0, the equilibrium anionic species are given by $3SiO_3^{2-} \rightleftarrows SiO_4^{4-} + Si_2O_5^{2-}$. In alkali-silicate melts with $NBO/Si \leqslant 1.3$ and in aluminosilicate melts with $NBO/T < 1.0$, where* T *is (Si + Al), the anionic species in equilibrium are given by $Si_2O_5^{2-} \rightleftarrows SiO_3^{2-} + SiO_2$. In multicomponent melts with compositions corresponding to those of the major igneous rocks, the anionic species are* TO_2, T_2O_5, T_2O_6, *and* TO_4, *and the coexisting polymeric units are determined by the second and third of these disproportionation reactions.*

Earlier models of the anionic species in silicate melts have been based on polymer theory (*1*) and gas chromatographic and mass spectrometric analyses of trimethylsilyl (TMS) derivatives of silicate glasses (*2*). Unfortunately, the results from TMS derivatives are internally inconsistent in that the bulk ratio of nonbridging oxygens to tetrahedrally coordinated cations (NBO/Si) calculated from such data is lower by 25 percent or more than the theoretical values. Moreover, polymer theory does not take into account the effect of metal cations that control the types of anionic structures in silicate minerals (*3*). Models of melt structure based on these methods may, therefore, require reevaluation.

Vibrational spectroscopy, in particular the Raman technique, has proved very useful for the identification of distinct anionic species in silicate melts and glasses (*4–8*). Although a rigorous analysis of vibrational spectra of glasses is difficult, a useful approximation can be derived from a consideration of the vibrations of silicate anions only, not the vibrations of the network-modifying cations. With further extension of this approximation, specific anionic units in silicate glasses and melts can be identified by recognition of the distinct vibrational modes that are associated with $Si\text{-}O^-$ nonbridging bonds.

We have used Raman spectroscopy to determine the coexisting anionic species in silicate melts of most of the end-member mineral compositions quenched at 1 atm and other relevant binary and ternary joins of petrologic interest. From a synthesis of these data a comparatively simple structural model of the major polymeric units in multicomponent melts can be formulated. A summary of the proposed structural model is presented here.

In Table 1 are listed the Raman frequencies of the Si-O stretching bands and the range of the band positions as a function of NBO/Si that have been identified in the Raman spectra of chemically different silicate melts. The assignment of the distinct groups of frequencies to SiO_4 tetrahedra containing, on the average, 0, 1, 2, 3, and 4 NBO/Si (Table 1) is based on comparisons of the Raman spectra of isochemical crystals of end-member mineral compositions (*4–6, 9*) as well as theoretical calculations of the Raman spectra of $Si_2O_5^{2-}$ sheet and SiO_3^{2-} chain species (*4, 10*) and SiO_2 three-dimensional melt structures (*11*). It is stressed that, in the various chemical systems that have been studied, no resolved bands corresponding to other anionic units have been found in the polarized Raman spectra of silicate melts in addition to those listed in Table 1. The assignment of bands to linear trimers, tetramers, pentamers or other species (*1, 2*) can thus be eliminated, as such units will result in symmetric stretch bands between 900 and 970 cm^{-1} (different NBO/Si) where no Raman bands are found (see Table 1 and Fig. 1). There is a small but systematic variation of the band positions for specific anionic units as a function of NBO/Si (Table 1), but this variation is directly correlated with changes in the relative intensities of the bands (Fig. 1). It is unlikely, therefore, that such a variation in band position mandates different band assignments.

In connection with the chain units designated in Table 1, it is not possible to differentiate between infinite chains as in metasilicate crystals and ring structures with NBO/Si = 2.0 (*12*). On the basis of calculations of the degree of localization of vibration modes associated with nonbridging oxygens (*10, 13*), however, it can be suggested that the $(SiO_3)_n^{2n-}$ unit (Table 1) refers to linear chains with $n \geqslant 10$ or groups of rings with $n \geqslant 3$. Also in connection with the assignment of the band in the region 1050 to 1100 cm^{-1}, we note that branching or multiplication of chains can result in sheets. In fact, polymer theory (*1*) predicts that the extent of branching increases as a function of decreasing metal/silica (*M*/Si). The frequency of this band is almost invariant of *M*/Si in specific chemical systems, however, and this invariance indicates that increased branching does not take place. Branched chains are also unlikely in view of the fact that, presumably for energetical reasons, such structures are not found in silicate minerals (*3*). On the basis of Raman spectroscopy alone, we cannot rule out that the band at 1050 to 1100 cm^{-1} is due to multiple chains (finite sheet). However, in view of the similarity in frequency and polarization characteristics of this band to those of the symmetric stretch band in sheet silicates (*4*), an infinite sheet interpretation is favored. In the following discussion the band assignments listed in Table 1 are used for the sake of simplicity.

The Raman spectra (*14*) of quenched melts with compositions along the CaO-SiO_2 join and in the range NBO/Si = 1.0 to 2.8 are given in Fig. 1. The range of melt compositions that have been studied in this system is restricted by the high liquidus temperatures (> 1700°C) of the *M*O-rich compositions and by liquid immiscibility of the SiO_2-rich composition (*15*). The range of melt compositions that have been studied in other binary and ternary systems is also restricted for similar reasons and because of the hygroscopic nature of alkali-silicate melts with NBO/Si > 2.0. The dominant features of each spectrum (Fig. 1) are the intense, slightly asymmetric band in the region 593 to 650 cm^{-1} and the intense high-frequency envelope in the region 800 to 1100 cm^{-1}. All these bands are strongly polarized. The resolved high-frequency bands (Fig. 1) due to $Si\text{-}O^-$ symmetrical stretch vibrations are assigned to specific anionic units according to the summary in Table 1. These assignments are SiO_4^{4-} monomer (830 to 869 cm^{-1}), $Si_2O_7^{6-}$ dimer (905 to 927 cm^{-1}), SiO_3^{2-} chain (955 to 963 cm^{-1}), and $Si_2O_5^{2-}$ sheet (1058 to 1057 cm^{-1}). The presence of the band assigned to the $Si_2O_5^{2-}$ sheet unit in the spectrum of the metasilicate composition is clearly justified by the increased intensity of this band in the melts with lower NBO/Si (Fig. 1). The inferred absence of the dimer unit in the metasilicate melt is further substantiated from the spectra of alkali-metasilicate melts (*4, 8*). In alkali-silicate melts the bands assigned to the monomer, chain,

0036-8075/80/0620-1371$00.50/0 Copyright © 1980 AAAS

Table 1. Raman frequencies of the stretch vibrations of specific silicon-rich anionic units in melts.

Structural unit*	O^-/Si	Frequency† (cm^{-1})	Characteristics of the vibrational mode‡
SiO_4^{4-}	4	850 to 870	s, p; symmetrical stretch
$Si_2O_7^{6-}$	3	905 to 920	s, p; symmetrical stretch
SiO_3^{2-}	2	970 to 950	s, p; symmetrical stretch
$Si_2O_5^{2-}$	1	1050 to 1100	s, p; symmetrical stretch
SiO_2	0	1065, 1200	vw, dp; antisymmetrical stretch

*See text for further discussion. †The trend in frequency for the different depolymerized anionic units is listed as a function of decreasing NBO/Si. This trend is similar in systems with different network modifiers. ‡Abbreviations: s, strong; vw, very weak; p, polarized; dp, depolarized.

and sheet units are completely resolved because of the smaller band widths as compared with the spectra in the system $CaO-SiO_2$. In the above interpretation the intense low-frequency band (593 to 650 cm^{-1}) in each spectrum is composite where the Si-O-Si vibrations characteristic of the dimer, chain, and sheet units are not resolved.

The most important observation made from the above assignment of the Raman spectra is that there is a unique set of coexisting anionic species for specific ranges of NBO/Si. Values of this ratio for each melt composition are calculated on the assumption that Ca^{2+} is octahedrally coordinated in the melt structure as in the isochemical crystalline phases. For $CaO-SiO_2$ melts with $NBO/Si \gtrsim 2.0$, the coexisting species are SiO_4^{4-}, $Si_2O_7^{6-}$, and SiO_3^{2-}; in the range $NBO/Si = 1.0$ to 2.0, the equilibrium anionic species are SiO_4^{4-}, SiO_3^{2-}, and $Si_2O_5^{2-}$.

These conclusions are significant because a similar pattern of coexisting anionic species is also evident for melts quenched at 1 atm along relevant portions of the joins $CaMgSiO_4-SiO_2$ ($NBO/Si = 1.34$ to 3.86), $MgO-SiO_2$ ($NBO/Si = \sim 2.0$), K_2O-SiO_2 ($NBO/Si = 2.0$), Na_2O-SiO_2 ($NBO/Si = 1.33$ to 2.0), and Li_2O-SiO_2 ($NBO/Si = 1.33$) (4, 5, 8, 16).

In view of the similar results for melts with different network modifiers and because of mass balance considerations, we propose that, for melts with $NBO/Si > 2.0$, the three major anionic units are in equilibrium according to the disproportionation reaction of the type

$$Si_2O_7^{6-} \rightleftarrows SiO_4^{4-} + SiO_3^{2-} \quad (1)$$

In melts with $2 > NBO/Si \gtrsim 1.0$, the equilibrium is expressed in terms of the reaction

$$3SiO_3^{2-} \rightleftarrows SiO_4^{4-} + Si_2O_5^{2-} \quad (2)$$

It is to be expected, however, that structural units more polymerized than those occurring in Eq. 2 predominate in binary melts with compositions close to the SiO_2 composition. In systems such as $CaO-SiO_2$ and $MgO-SiO_2$, it is not possible to quench single-phase glasses with $NBO/Si \lesssim 1.0$ because of liquid immiscibility. In alkali-silicate melts such as K_2O-SiO_2, Na_2O-SiO_2, and Li_2O-SiO_2 it is observed in the Raman spectra that the band assigned to SiO_4^{4-} monomers is absent in melts in the range $\sim 1.0 < NBO/Si = 0$ (4, 5, 8); the bands assigned to the $Si_2O_5^{2-}$ sheet and SiO_3^{2-} chain are present. From mass balance considerations, the presence of a more polymerized anionic unit is mandated. The presence of anionic units with a three-dimensional network structure in addition to $T_2O_5^{2-}$ sheets and TO_3^{2-} chains in the spectra of highly polymerized M_2O-SiO_2 melts can be positively identified (4, 11). Similar results are also found for the highly polymerized aluminosilicate melts in the $CaMgSi_2O_6-NaAlSi_3O_8-CaAl_2Si_2O_8$, $CaMgSi_2O_6-NaAlSiO_4-SiO_2$, and $Mg_2SiO_4-NaAlSi_3O_8-CaAl_2Si_2O_8$ systems, with $NBO/T < 0.75$ (16).

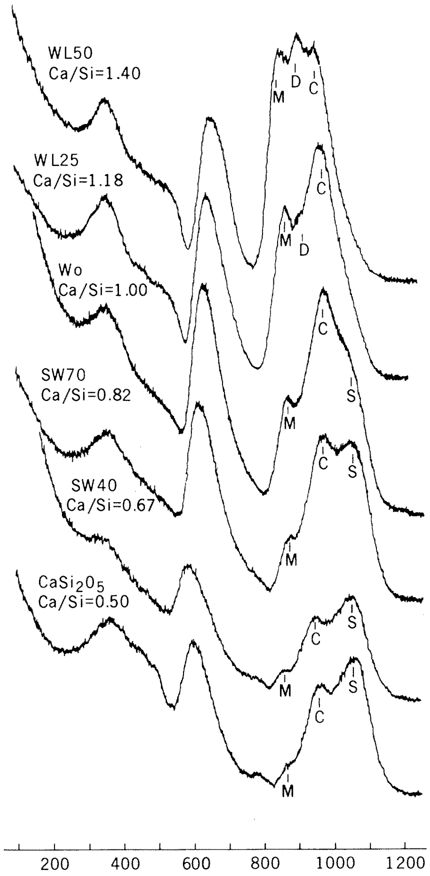

Fig. 1. Raman spectra of 1-atm glasses along the $CaO-SiO_2$ join; *M*, *D*, *C*, and *S* refer to monomer, dimer, chain, and sheet species, respectively.

In view of these results, we propose a third disproportionation reaction for melt compositions with $NBO/T \lesssim 1.0$:

$$T_2O_5^{2-} \rightleftarrows TO_3^{2-} + TO_2 \quad (3)$$

where T refers to Si for the alkali-silicate systems and to both Si and Al for the aluminosilicate melts.

The hypothesis proposed is that the chemical equilibria between the coexisting anionic species in various binary alkali and alkaline-earth silicate melts can be expressed in terms of disproportionation reactions 1, 2, and 3. The details of these reactions will also depend on pressure, temperature, and changes in the composition of the cation and the anion matrix.

A major question that remains unanswered concerns the relationship of the data on glasses to silicate melts. Experimental data pertaining to proof of the structural similarity between melts and their quenched analogs are comparatively few. On the basis of infrared and Raman spectra of 1-atm melts with compositions along the Na_2O-SiO_2 join (7, 8), however, it can be concluded that there are no discernible differences between the spectra of melt and glass. In addition, Taylor *et al.* (17) found that the structure of 1-atm $NaAlSi_3O_8$ glass is the same at temperatures above and below the glass transition temperature. We conclude, therefore, that the Raman data on glasses are applicable to molten silicates.

On the basis of the results presented here, the anionic species in 1-atm multicomponent silicate melts with compositions corresponding to those of the major igneous rocks can be predicted. The network-forming cations, T [= Si, Al^{3+}, Fe^{3+}, Ti^{4+}, and P^{5+}(16, 18)] can be expected to be distributed between TO_2, T_2O_5, T_2O_6, T_2O_7, and TO_4 polymeric units. In melts, trivalent cations will be charge-balanced by the formation of complexes of the types $Na(K)AlO_2$, $Ca(Mg)Al_2O_4$, and $Na(K)FeO_2$ (12, 15).

The calculated NBO/T for most alkali basalts, tholeiites, and more acidic rocks is generally < 1.0, whereas this ratio is between 1 and 2 for basanites and picrites. Thus, we propose that the equilibrium polymeric units in most igneous melts will be determined by disproportionation reactions 2 and 3.

D. Virgo
B. O. Mysen
I. Kushiro

Geophysical Laboratory,
Carnegie Institution of Washington,
Washington, D.C. 20008

References and Notes

1. P. C. Hess, *Geochim. Cosmochim. Acta* **35**, 289 (1971); C. R. Masson, *Proc. R. Soc. London Ser. A* **287**, 201 (1965).
2. C. W. Lentz, *Inorg. Chem.* **3**, 574 (1964); C. R. Masson, *J. Non-Cryst. Solids* **25**, 3 (1977); R. M. Smart and E. P. Glasser, *Phys. Chem. Glasses* **19**, 95 (1978).
3. L. S. Dent Glasser, *Z. Kristallogr.* **149**, 291 (1979).
4. S. A. Brawer and W. B. White, *J. Chem. Phys.* **63**, 2421 (1975).
5. W. L. Konijnendiijk, *Philips Res. Rep. Suppl.* 1 (1977).
6. H. Verweij, *J. Non-Cryst. Solids* **33**, 41 (1979); *ibid.*, p. 51.
7. J. R. Sweet and W. B. White, *Phys. Chem. Glasses* **10**, 246 (1969).
8. S. K. Sharma, D. Virgo, B. O. Mysen, *Carnegie Inst. Washington Yearb.* **77**, 649 (1978).
9. A. N. Lazarev, *Vibrational Spectra and Structures of Silicates* (Consultants Bureau, New York, 1964).
10. S. A. Brawer, *Phys. Rev. B* **11**, 3173 (1975).
11. F. L. Galeaner, *ibid.* **19**, 4292 (1979); P. N. Sen and M. F. Thorpe, *ibid.* **15**, 4030 (1977).
12. D. M. Adams and I. R. Gardner, *J. Chem. Soc. Dalton Trans.* **1974**, 1502 (1974); *ibid.* **1976**, 315 (1976).
13. R. J. Bell and P. Dean, in *International Conference on the Physics of Noncrystalline Solids, 3rd, University of Sheffield, 1970*, R. W. Douglas and B. Ellis, Eds. (Wiley-Interscience, London, 1972), pp. 443-452.
14. The Raman spectra were taken on small chips of glass (~0.5 mm). Experimental details are similar to those given by Sharma *et al.* (*8*).
15. The starting mixes were prepared from spectrographically pure oxides that were thoroughly mixed, melted, and quenched in molybdenum disilicate-wound vertical quench furnaces. For melt compositions along the Ca_2SiO_4-SiO_2 and $CaMgSiO_4$-SiO_2 joins, the oxide mixes were held at 1650°C for 1/2 hour in sealed platinum capsules. The capsules were quenched in water at a rate of about 500°C per second.
16. D. Virgo, F. Seifert, B. O. Mysen, *Carnegie Inst. Washington Yearb.* **78**, 502 (1979).
17. M. Taylor, G. E. Brown, P. H. Fenn, *Geochim. Cosmochim. Acta*, in press.
18. B. O. Mysen, F. Seifert, D. Virgo, *Am. Mineral.*, in press; B. O. Mysen, R. Ryerson, D. Virgo, *ibid.*, in press.

27 March 1980

Spaceborne Imaging Radar: Monitoring of Ocean Waves

Abstract. *A well-organized, very low energy ocean swell system off the East Coast of the United States was tracked with the Seasat synthetic aperture radar from deep water, across the continental shelf, and into shallow water. The results indicate that spaceborne imaging radar may be used to accurately measure ocean wavelength and direction, even in coastal areas and in the presence of a mixed ocean.*

A number of aircraft studies in the past few years have indicated that ocean swell can be imaged with synthetic aperture radar (SAR), at least for some values of wind velocity when there is a substantial component of the swell traveling along the line of sight of the radar (*1*). The bounds of wind, wave, and geometric conditions over which reliable ocean wave detection occurs, however, remain elusive for want of an extensive experimental data base. Seasat provided a unique, although limited, opportunity to reexamine the wave detection problem without some of the artificial constraints of aircraft measurements. A concise summary of the Seasat SAR design parameters and a more general description of the total Seasat SAR system and some of its fundamental information limitations have been given in (*2*). A preliminary assessment of the Seasat SAR ocean wave detection capabilities has been compiled in (*3*).

During the limited 100-day lifetime of the Seasat SAR, data from more than 400 passes of duration ranging from 1 to 15 minutes were collected at three domestic and two foreign receiving stations. About 20 of these passes provided acceptable SAR imagery within 70 km of a well-instrumented "sea truth" pier operated by the U.S. Army Corps of Engineers, Coastal Engineering Research Center (CERC) at Duck, North Carolina. The Applied Physics Laboratory of the Johns Hopkins University, along with several government agencies, collected a variety of wind and wave measurements during a concentrated 8-week period from 12 August to 9 October 1978.

On the morning of 28 September 1978, at 1520 G.M.T., Seasat approached the East Coast of the United States, with the SAR 100-km swath running approximately parallel to the coast but displaced eastward by about 20 km. On the basis of the present analysis of that pass, several major conclusions may be reached:

1) The SAR can successfully detect low-energy swell systems of significant wave heights, H_s, well under 1 m (actually 0.65 ± 0.25 m), at least for surface windspeeds (normalized to 10 m above sea level) of 2 m/sec $\leqq U_{10} \leqq$ 10 m/sec.

2) Refraction of low-energy but well-organized swell due to local changes in ocean depth is clearly detectable in wavelength.

3) The complexity of the ocean spectrum (for example, whether it is composed of more than one system or is spread in direction and wave number) seems to have little bearing on the threshold detection limits.

Figure 1 identifies the various regions off the East Coast for which estimates or measurements of wind and waves were collected on the morning of 28 September. For reference, the edges of the 100-km SAR swath are shown by the solid lines inclined at approximately 23° with respect to north at this latitude. The locations are keyed in alphabetical order from north to south. Location A corresponds to the Navy Fleet Numerical Weather Central (FNWC) grid point 271. Locations B, C, E, and F are areas, each 15 km square, over which the Seasat SAR imagery was optically Fourier-transformed. The local ocean depth (shown with dashed contours in Fig. 1) changes appreciably over the 15-km square at locations B, C, and E, which would cause appreciable spreading of a single-frequency, deep-water wave in both wavelength and direction. Deep-water dispersion prevails only at location F for wavelengths greater than 70 m. Local depth changes at location B are especially severe, ranging from less than 10 m to at least 20 m. The National Oceanic and Atmospheric Administration (NOAA) Sea Air Interaction Laboratory aircraft laser profilometer was operating at location E. In situ, one-dimensional spectral measurements were collected at the CERC pier (location D). The FNWC grid point 260 is represented by location

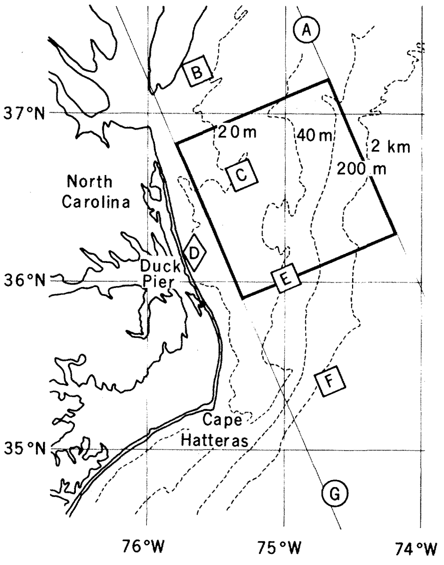

Fig. 1. Locations of surface, aircraft, and spacecraft measurements of the low-energy swell systems present on 28 September 1978. The cover image is located by the 100-km square centered at 36.5°N and 75.1°W.

0036-8075/80/0620-1373$00.50/0